https://doi.org/10.5194/egusphere-2025-659
Preprint. Discussion started: 31 March 2025

Numerical modeling of the tipping processes of ice detachment: a case study of Sedongpu Glacier in the Southeastern Tibetan Plateau

Tong Zhang[1, 2], Wei Yang[2], Yuzhe Wang[3], Chuanxi Zhao[4], Qingyun Long[1], and Cunde Xiao[1]

[1]State Key Laboratory of Earth Surface Processes and Hazards Risk Governance, Beijing Normal University, Beijing, China, 100875
[2]State Key Laboratory of Tibetan Plateau Earth System, Environment and Resources (TPESER), Institute of Tibetan Plateau Research, Chinese Academy of Sciences, Beijing, 100101, China
[3]College of Geography and Environment, Shandong Normal University, Jinan, China, 250014
[4]School of Water Conservancy and Environment, University of Jinan, Jinan, China, 250001

Correspondence: Tong Zhang (tzhang@bnu.edu.cn) and Wei Yang (yangww@itpcas.ac.cn)

Abstract. Glacier detachment is a severe natural hazard that can cause enormous damage in downstream regions. During the detachment, glacier will experience an abrupt change from slow-moving to high-speed flow in just a few minutes. In this study, we investigate a massive glacier detachment event occurred in 2018 at the Sedongpu valley, Southeastern Tibet, using a two-dimensional first-order ice flow model by introducing an ice stiffness and basal slip positive feedback mechanism. In this model approach, ice detachment can be triggered if ice stress exceeds the initial yield strength of the glacier. By including this tipping mechanism, we simulate the abrupt changes in the ice flow pattern for the Sedongpu glacier. The transition process from slow to abrupt flow can occur within just several model time steps. The modeled duration time of the 2018 Sedongpu detachment is comparable with observation. The abrupt weakening of ice strength from elastic to plastic deformation may be one of the main causes of the tipping processes of glacier detachment. This numerical model approach could possibly be used for early warnings of glacier detachment hazards in the surrounding regions of the Sedongpu valley.

1 Introduction

Glacier avalanche/detachment is one of the most catastrophic natural disasters in mountainous region and serves as clear evidence of tipping elements in the cryosphere. In recent years, the global warming trend has intensified, leading to an increasing occurrence of glacier instability and a higher probability of ice avalanche/detachment disasters, posing significant safety risks to downstream populations and infrastructure (Acharya et al., 2023; Zhang et al., 2024).

For example, in 1950s, the Zelongnong and Guxianggou ice avalanches occurred, causing a river blockage chain disaster in Tibet (Hu et al., 2018). In 1962, the Huascaran ice avalanche and subsequent debris flow created a disaster in the Andes Mountains in Peru (Salzmann et al., 2004). In 2002, the Kolka ice avalanche triggered a mudslide disaster in Russia (Kotlyakov et al., 2004). Between 2009 and 2016, the ice avalanche-rockfall events occurred in the Siachen Glacier, Himalaya, resulting in several fatalities (Berthier and Brun, 2019). In 2016, twin glaciers collapsed massively in Aru, Tibet (Gilbert et al., 2018; Kääb et al., 2018). Notably, in October 2018, the Sedongpu glacier detached, releasing nearly 130 million m^3 of ice-debris

https://doi.org/10.5194/egusphere-2025-659
Preprint. Discussion started: 31 March 2025

mass downstream, marking the largest ever recorded event. This led to the blockage of the Yarlung Tsangpo River for two days, posing a flood threat to the downstream regions in Bangladesh (Li et al., 2022).

Recently, advances in glacier avalanche/detachment studies have been driven by remote sensing and field observations. Satellite-based synthetic aperture radar (SAR) and optical remote sensing have been utilized to map surface velocities and detect changes in surface features, such as crevasses and fractures, which can indicate the potential occurrence of ice avalanches (Luo et al., 2022; Ding et al., 2023). Additionally, the use of unmanned aerial vehicles (UAVs) has allowed researchers to collect high-resolution imagery and data in previously inaccessible areas, providing insights into glacier dynamics and avalanche/detachment processes (Fugazza et al., 2018; Gao et al., 2023).

However, the dynamic mechanism that induces ice avalanche/detachment remains unclear. Previously, Gilbert et al. (2020) and Kääb et al. (2018) concluded that, among a combination of climatological, glaciological and geomorphologial triggers, the deformable bed and changes of basal friction were important factors responsible for the Aru ice avalanches. Later, Bai and He (2020) applied observed seismic waves to estimate glacier motion parameters and simulate the extent of the Aru avalanche. But there still lacks a clear and in-depth numerical and physical explanations of the abrupt, transient behavior of glacier detachment. This presents a significant challenge in building an effective early warning system for damage control and management.

To further our understanding of the glacier detachment mechanism, we study the 2018 Sedongpu glacier detachment in this paper. Firstly, we describe the environmental conditions of the study site. Then, we introduce the numerical model methods we used, where a noval ice stiffness-basal slip postive feedback coupling scheme is implemented, following by the results and discussions. Finally, we present our conclusions at the end of the paper.

2 Study region

The study area is situated within the Namcha Barwa-Gyala Peri massif in the southeastern Tibetan Plateau (Fig. 1a), characterized by several distinctive features, including high tectonic activity, significant variations in topography and deep incisions caused by the Yarlung Tsangpo River. The Indian summer monsoon penetrates through the Yarlung Tsangpo Canyon, resulting in the longest annual rainy season on the Tibetan Plateau (Yang et al., 2013). In 2019–2020, Medog, located about 60 kilometers from the Sedongpu Valley, received over 1200 millimeters of precipitation, with 56.6% occurring from June to September and 32.4% in the spring season (March-May) (Li et al., 2022) .

As a result, the abundant monsoonal rainfall has led to the presence of 141 modern temperate glaciers in the Namcha Barwa-Gyala Peri region. Additionally, the accumulation of thick Quaternary glacial deposits (Montgomery et al., 2004), along with these unique climatic, and topographic conditions have historically resulted in significant natural disasters and river blockages (Chen et al., 2020).

According to the Randolph Glacier Inventory (RGI) 6.0 , the Sedongpu valley is home to five major glaciers. The largest of these is the Sedongpu Glacier (RGI60-13.01428), covering an area of 5.0 km^2, the majority of which detached in October 2018 (Kääb et al., 2021). The glacier surface is heavily covered with debris, while the underlying bedrock primarily consists of Proterozoic marble and gneiss (Chen et al., 2020).

https://doi.org/10.5194/egusphere-2025-659
Preprint. Discussion started: 31 March 2025

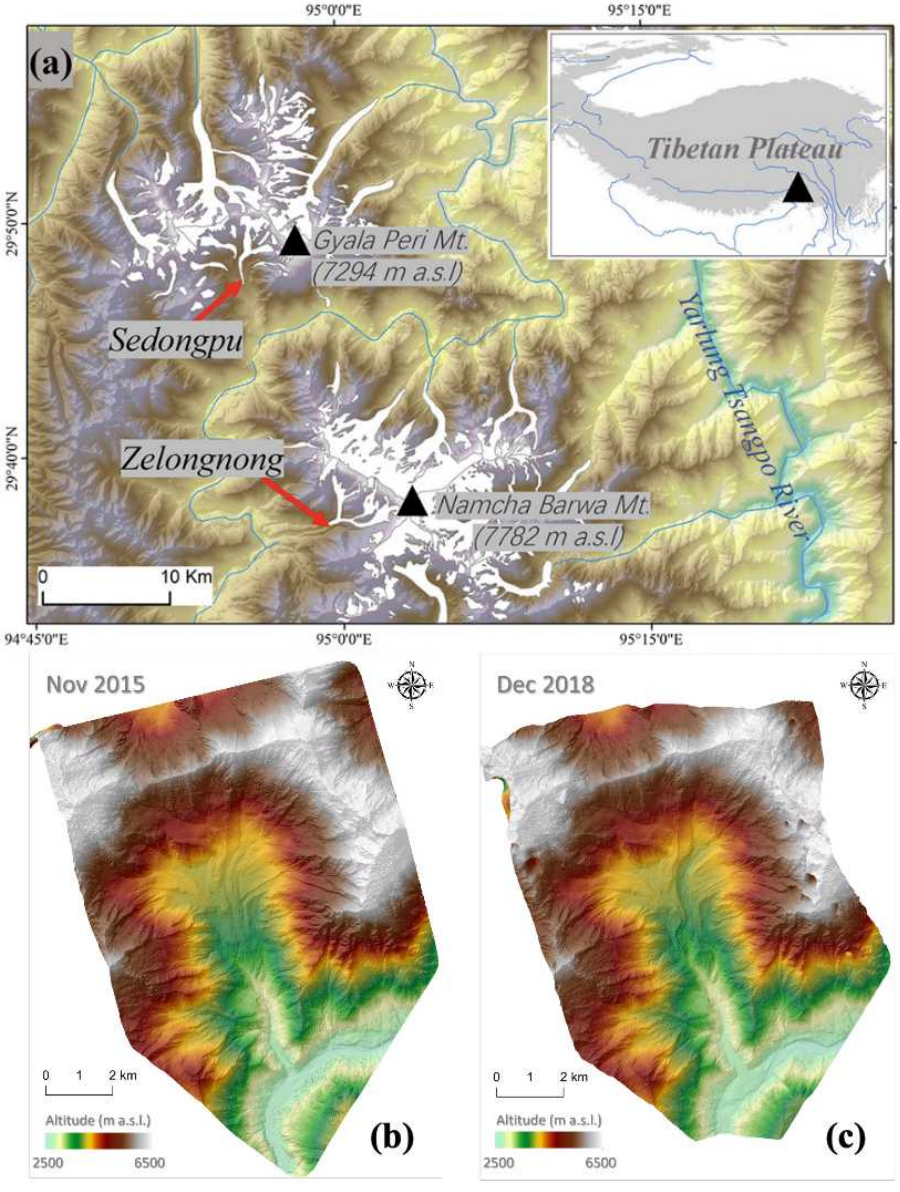

Figure 1. The location of Sedongpu valley and the glacier distribution around Namcha Barwa Mt and Gyala Peri Mt. (a). High-resolution DEMs generated from the stereo optical satellite images in November 2015 (b) and December 2018 (c) showing the surface and bed topography before and after the glacier detachment in 2018. The DEM difference between 2015 and 2018 can be seen in Figure 3a.

https://doi.org/10.5194/egusphere-2025-659
Preprint. Discussion started: 31 March 2025

3 Model descriptions

3.1 Ice flow model

In this study, we use a two-dimensional high-order ice flow model named as PoLIM (Polythermal Land Ice Model) (Zhang et al., 2013; Wang et al., 2018, 2020). PoLIM is developed according to the hydrostatic approximation, where the horizontal gradient of the vertical velocity is neglected in the viscous rheology and momentum equation (Blatter, 1995; Pattyn, 2002; Greve and Blatter, 2009). The momentum conservation equation of PoLIM is given by:

$$\frac{\partial}{\partial x}(2\tau_{xx}+\tau_{yy})+\frac{\partial \tau_{xy}}{\partial y}+\frac{\partial \tau_{xz}}{\partial z}=\rho_i g\frac{\partial s}{\partial x}, \tag{1}$$

where x represents the streamline direction, y represents the transverse direction, and both x and y axes lie in the horizontal plane, while z represents the vertical direction, and s represents the surface elevation of the glacier. In addition, ρ_i represents the ice density, and g represents the acceleration due to gravity. Finally, τ_{ij} is the component of the deviatoric stress tensor, which can be calculated from the strain rate

$$\tau_{ij}=2\eta\dot{\epsilon}_{ij}, \tag{2}$$

where $\dot{\epsilon}_{ij}(i,j=1,2,3)$ are the corresponding strain-rate components, and η is the effective viscosity, calculated as:

$$\eta=\frac{1}{2}A^{-1/n}\dot{\epsilon}_e^{(1-n)/n}, \tag{3}$$

where n is the flow law exponent and the effective strain rate $\dot{\epsilon}_e$ is defined as

$$\dot{\epsilon}_e\equiv\left(\dot{\epsilon}_{11}^2+\dot{\epsilon}_{22}^2+\dot{\epsilon}_{11}\dot{\epsilon}_{22}+\dot{\epsilon}_{12}^2+\dot{\epsilon}_{13}^2+\dot{\epsilon}_{23}^2\right)^{\frac{1}{2}}. \tag{4}$$

In this study, we assume Sedongpu glacier is temperate and set A as a constant. At the glacier surface, we use a stress-free boundary condition, and at the glacier base, we apply a linear friction law prior to the occurrence of glacier detachment,

$$\tau_b=\beta u_b, \tag{5}$$

where τ_b is the basal stress, u_b is the basal sliding speed, and β is the basal friction parameter. The glacier evolution is described by the mass continuity equation,

$$\frac{\partial H}{\partial t}=-\frac{\partial(\bar{u}H)}{\partial x}+m_s, \tag{6}$$

where H is ice thickness, t is model time, $\bar{u}$ is depth-averaged velocity, and m_s is surface mass balance. Here we set model time step to 1 second, and set m_s to 0 given a very short model time span (25 minutes) in this study. We use a $\Delta x=48$m in x and 20 vertical layers in z with a terrain-following coordinate. All model constants and parameters can be found in Table 1.

From the model descriptions above, we can see that glacier movement consists of two components: internal deformation and basal sliding. Internal deformation is influenced by ice viscosity. Decreased viscosity lead to increased ice flow. The basal sliding is controlled by the friction at ice-bed interface. Factors such as soft sediments and basal meltwater lubrication will reduce the basal friction, consequently accelerating ice flow.

https://doi.org/10.5194/egusphere-2025-659
Preprint. Discussion started: 31 March 2025

Table 1. Model parameters and constants used in our experiments

Symbol	Description	Value	Units
ρ_i	ice density	910	kg m^{-3}
g	gravitational constant of acceleration	9.81	m s^{-2}
n	flow law exponent	3	
A	rate factor	10^{-16}	Pa^{-n} yr^{-1}
ϵ_c	critical strain	0.1	
τ_c	intact strength of ice	5×10^6	Pa
C	friction coefficient	4×10^6	Pa (s/m)$^{1/n}$
p	step-size parameter	1.5	
Δt	model time step	1	s

3.1.1 Model initialization prior to detachment

Before simulating the Sedongpu detachment processes, we need to initialize the ice flow model using observed ice surface velocity data. Following Arthern and Gudmundsson (2010) and Arthern et al. (2015), we solve the basal friction coefficient using the Robin inversion algorithm by iteratively minimizing the cost function J across the basal domain

$$J = \int_{\Gamma_b} \beta \left| \boldsymbol{u}^D - \boldsymbol{u}^N \right|^2 \, \mathrm{d}S, \tag{7}$$

where $\boldsymbol{u}^D$ and $\boldsymbol{u}^N$ are the observed (Dirichlet-type) and modeled (Neumann-type) ice surface velocities, respectively. This cost function represents the mismatch between the Neumann and Dirichlet velocity fields. According to Arthern et al. (2015), the basal friction coefficient was updated as follows,

$$\beta_{i+1}(x,y) = \beta_i(x,y) + \alpha_\beta \left(\left| \mathbf{u}_b^N \right|^2 - \left| \mathbf{u}_b^D \right|^2 \right), \tag{8}$$

where β_i is the basal friction at the i-th iteration step, $\mathbf{u}_b^N$ and $\mathbf{u}_b^D$ are basal velocity for Neumann and Dirichlet iterations, α_β is a positive parameter that determines the step size, given as

$$\alpha_\beta = \frac{\beta_n}{\left| \mathbf{u}_b^D \right|^p} \frac{\left(\left| \mathbf{u}_b^N \right|^p - \left| \mathbf{u}_b^D \right|^p \right)}{\left(\left| \mathbf{u}_b^N \right|^2 - \left| \mathbf{u}_b^D \right|^2 \right)}, \tag{9}$$

where p is a positive parameter, as given in Table 1.

3.2 Yield strength and basal slip coupling scheme

In order to simulate the tipping mechanism of Sedongpu detachment, we implement a numerical scheme that couples basal slip and ice stiffness, following the approach in Bassis et al. (2021), which integrates the continuum and discrete processes of ice

https://doi.org/10.5194/egusphere-2025-659
Preprint. Discussion started: 31 March 2025

flow. In this scheme, the ice viscosity is calculated as

$$\eta = \eta_{\min} + \left[\frac{1}{\eta_1} + \frac{1}{\eta_2} + \frac{1}{\eta_3}\right]^{-1}, \tag{10}$$

where η_1, η_2 and η_3 are the viscosity for diffusion creep, Glen's pow law creep flow and plastic deformation when ice failure occurs. $\eta_{\min}$is a tunable minimum viscosity for numerical stability. The inclusion of the viscosity η_3 in the fracture process indicates that stress does not increase with increasing strain when the ice mass reaches the yield stress,

$$\eta_3 = \frac{\tau_y}{2\epsilon_e}, \tag{11}$$

where τ_y is the yield strength of ice.

The presence of a "plastic" viscosity results in a low stiffness value and high velocity, as the ice viscosity remains relatively low. This phase corresponds to the development of ice crevasses and prevalent ice failure in reality. Additionally, the yield strength is not stable and constant; it decreases with the acceleration of ice flow, resulting in an unstable ice flow pattern,

$$\tau_y = \max\left\{\tau_c - (\tau_c - \tau_{\min})\frac{\epsilon_p}{\epsilon_c}, \tau_{\min}\right\}, \tag{12}$$

where τ_c is the intact strength (see Table 1), $\tau_{\min}$ is a tunable, prescribed minimum yield stress, ϵ_c is the critical strain, and ϵ_p is the plastic strain accumulated in faults and fractures which can be calculated during the model run. For the basal sliding law, we also consider the impact of yield strength of basal ice, according to Bassis et al. (2021),

$$\tau_b = -\{\frac{1}{C u_b^{1/n-1}} + \frac{u_b}{\tau_y}\}^{-1} u_b, \tag{13}$$

where τ_b and u_b are basal stress and speed, respectively, and C is a constant. With this improvement, basal slip is enhanced as ice failure increases and basal ice strength decreases. Therefore, this mechanism can better capture the dynamics of the soft and thick till layer underneath Sedongpu glacier, which could deform significantly during detachment (Yang et al., 2023).

In Figure 2, we present a diagram of our numerical modeling processes. In the traditional ice flow framework (Glen's flow law), an increase in stress strengthens viscosity during the elastic phase of ice deformation, which tends to maintain slow and stable ice flow. However, for basal sliding, the basal friction is related to velocity and stress but does not consider ice stiffness (e.g., the Weertman sliding law), which limits the simulation of ice detachment.

The model framework we propose here incorporates the plastic phase of ice flow by introducing the tipping point of yield stress, thus involves two positive dynamic feedback mechanisms in internal ice deformation and basal sliding. On one hand, when the ice strength reaches a threshold, both the ice stiffness and yield stress decrease, leading to more ice yielding and increasing the vulnerability of the glacier. On the other hand, as the basal ice stiffness decreases, basal friction also decreases, making the glacier easier to slide and accelerate.

4 Datasets

Glacier topography: We generated two high-resolution digital elevation models (DEMs) using commercial stereo optical satellite images: a 1-meter-resolution SPOT6 image captured on November 13, 2015, and a 0.5-meter-resolution Pleiades-1A image

https://doi.org/10.5194/egusphere-2025-659
Preprint. Discussion started: 31 March 2025

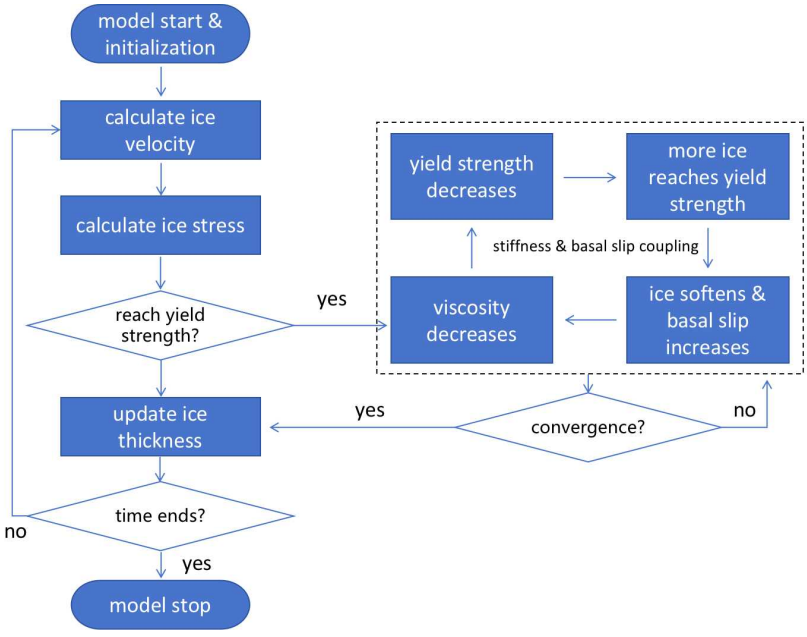

Figure 2. The flow diagram of the numerical modeling procedures in this study.

captured on December 30, 2018. These images were processed in PCI Geomatica software (Banff Service Pack 4) with the OrthoEngine module. The ice below 4300 m a.s.l. of Sedongpu Glacier was completely detached in October 2018 , exposing the underlying bed (Li et al., 2022; Kääb et al., 2021). Therefore, the December 2018 DEM represents the bed topography, and the November 2015 DEM is assumed to represent the surface topography. The final DEM difference products had a relative mean vertical accuracy of 1.3±3.2 m from November 2015 to December 2018 over stable flat ground inside the Sedongpu valley (Fig 3a).

We extracted the elevation differences at points where ice was substantially detached from the main glacier body. These elevation differences were assumed to provide a first-order estimate of ice thicknesses. We then estimated the distributed ice thickness of Sedongpu Glacier using GlaTE software, which infers thickness distribution by combining measured ice thickness and glaciological modeling results. Here, the discrete thickness data were regarded as measurements to constrain GlaTE. A glacier centerline was generated using the method proposed by Kienholz et al. (2014). Subsequently, we extracted the ice thicknesses along the centerline as input for PoLIM.

Ice surface velocity: we generated a spatially distributed estimate of XY surface displacements by applying a Normalized Cross Correlation algorithm to two phases of 3-meter Planet Labs optical satellite data in daily resolution (5 June 2018 and 18 September 2018) using ImGRAFT (Messerli and Grinsted, 2015) (Fig 3b). A search window of 10×10 pixels (30×30 m) was used to compute the magnitude and directions of the displacement vectors. Surface velocities greater than 400 cm/day were considered as noise and were filtered out, we interpolated the velocity values in the data gaps using cubic spline interpolation (Mishra et al., 2022).

https://doi.org/10.5194/egusphere-2025-659
Preprint. Discussion started: 31 March 2025

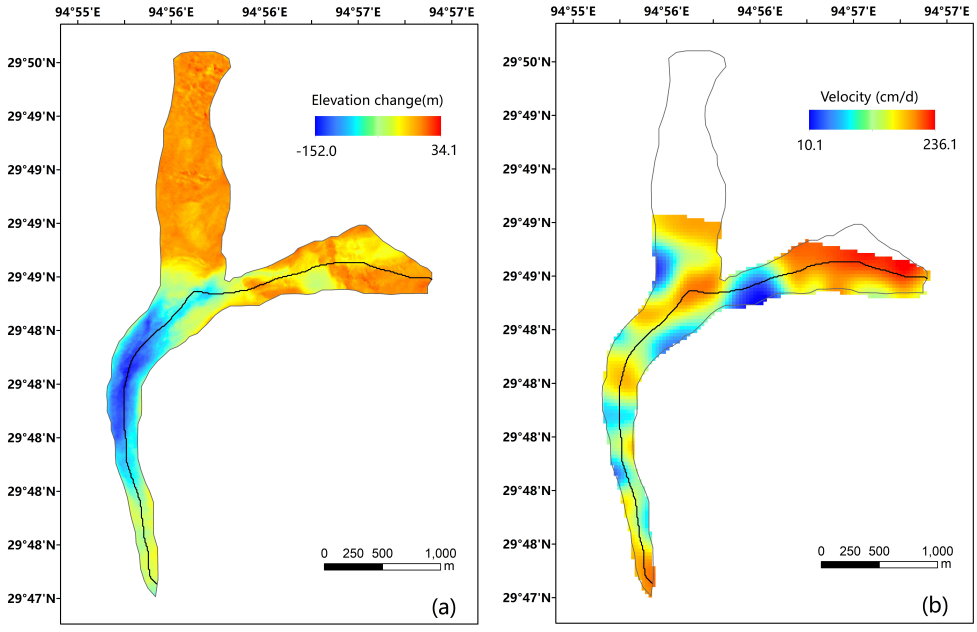

Figure 3. Ice surface elevation changes during 2015-2018 (a); Ice surface mean speed from June to September, 2018, prior to the ice detachment occurrence (b). The solid black curve represent the center flowline we use in this study.

5 Results and Discussions

5.1 Model initialization

The 2018 Sedongpu Glacier detachment occurred on October 17th. Prior to that, several ice-rock avalanches occurred at the top region of the glacier between June 2014 and October 2017, causing the ice flow increase from around 0.3 m/d in 2017 to 25 m/d at September, 2018 (Kaab et al., 2021). Due to a lack of high resolution observation data, it is difficult to simulate the speed-up processes of Sedongpu Glacier during this period. Therefore, to simulate the 2018 Sedongpu Glacier detachment, we initialize our model using the observed mean ice velocity from 2015 to 2018, before the detachment occurred. As shown in Figure 4, we inverted the basal sliding coefficient and internal velocity distribution features of the Sedongpu Glacier. We observe that, during this period, the Sedongpu Glacier flows faster at the upstream region where the basal friction is small, possibly due to a larger slope there. In contrast, in the downstream region where ice thickness is relatively large, the ice speed is low due to higher basal friction.

https://doi.org/10.5194/egusphere-2025-659
Preprint. Discussion started: 31 March 2025

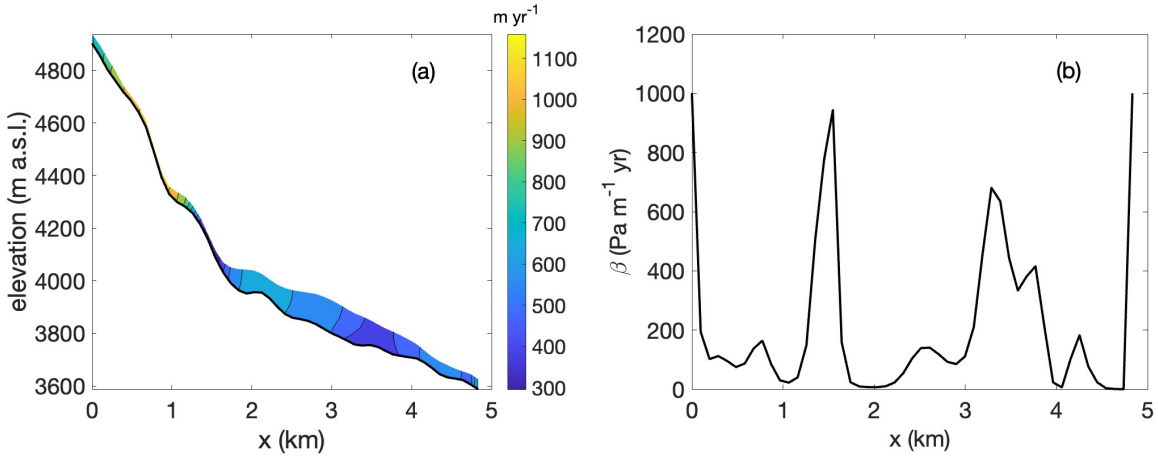

Figure 4. The ice velocity distribution along the main flow line (a) and the inverted basal sliding parameter using the Robin inversion algorithm (b).

5.2 Sedongpu detachment simulation

The external environmental forcings might be responsible for the 2018 Sedongpu detachment. In 2018, the increasing rate of historical mean temperature from January to October in the region was 0.039 K yr^{-1} (Liu et al., 2019) . Although the precipitation from January to October in 2018 over the Sedongpu region was lower than usual observations, there was intensified rainfall 2-4 days prior to the detachment, which may have softened the glacier and accelerate the ice flow, inducing changes in internal ice dynamic processes and leading to the abrupt ice collapse event. As shown in Figure 5, we are able to simulated the rapid detachment of the Sedongpu Glacier. We activated the yield strength and stiffness-slip coupling mechanism at $t_0 = 5$ minutes, and ran our model for 25 minutes. Within several model time steps, the overall mean viscosity of the Sedongpu Glacier decreased to its minimum value ($\eta_{\min}$), resulting in a significant increase in ice flow fluidity. Consequently, the ice velocity rapidly increased, from less than 1 m per hour to around 90,000 m per hour, with a mean speed of approximately 34,000 m per hour over the 25-minute simulation period. As the glacier quickly lost its mass and thinned, the ice speed stabilized at a low value, reaching a steady state as a result.

As shown in Figure 5, the mean effective stress of the Sedongpu Glacier drastically increases from 200 KPa prior to detachment to around 1000 KPa as ice flow accelerates after the detachment starts. Generally, the changes in englacial stress follow a similar pattern to that of ice speed. During the model run, the glacier mass is rapidly transported from upstream to downstream, resulting in a reduction in glacier thickness by approximately 80% within only 6.3 minutes and 90% within 11 minutes (Figure 5). Note that the oscillation of speed and effective stress after collapse is related to the prescribed minimum ice thickness (1 m) in our simulations: this unnatural model setting can produce non-smooth distributions in ice thickness, and thus speed and stress, correspondingly. Our model results closely match a previous estimation from October 17, 2018: the total detachment time lasted around 6.7 minutes and the mean ice speed was approximately 20 m s^{-1} (72,000 m per hour) (Liu et al., 2019).

https://doi.org/10.5194/egusphere-2025-659
Preprint. Discussion started: 31 March 2025

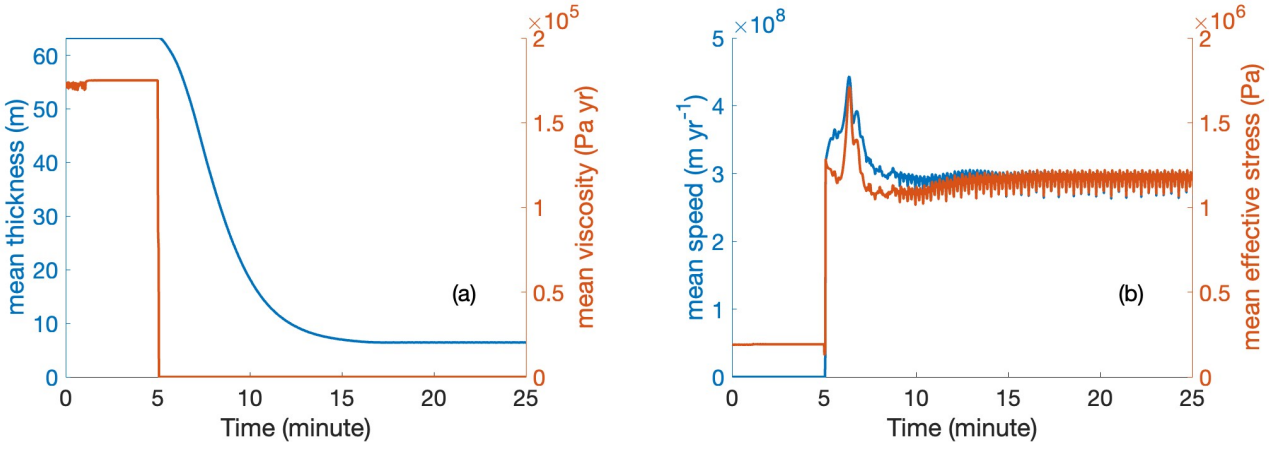

Figure 5. The transient changes of mean ice thickness, viscosity (a), ice speed and effective stress (b) in time for the Sedongpu glacier during a 25-minute model run. The detachment begins at minute 5. All variables here are shown in their normalized form in time.

5.3 Model sensitivity

In this study, we assume a spatially uniform yield strength at the model initialization (hereafter defined as "initial yield strength") across the Sedongpu Glacier. The initial yield strength of the glacier is a crucial parameter that determines the abrupt glacier detachment. As it generally varies widely within the range of 100–1000 KPa (Cuffey and Paterson, 2010), we conducted a series of sensitivity experiments on glacier dynamics to assess the impact of initial yield strength. This allows us to estimate the destablizing threshold (tipping point) for the Sedongpu Glacier. As seen in Figure 6a, we tested initial yield strength values ranging between 300 and 500 KPa. Clearly, the Sedongpu detachment is not triggered until we set the initial yield strength to be less than 440 KPa. This means that the mechanical properties of glacier ice might be determining in affecting the sudden collapse of a glacier when the ice failure exceeds some critical threshold. While a subglacial hydrology and ice dynamics coupling scheme can well explain the mechanism of glacier surge (Thøgersen et al., 2019), it is unlikely to be able to reproduce the extreme instability and tipping processes of glacier detachment without considering the dramatic weakening of ice strength, as suggested by the case of initial yield strength larger than 450 KPa in Figure 6a (glacier ice remains intact during the model simulation).

Additionally, the rate of ice loss can be significantly influenced by two tuning parameters, $\tau_{\min}$ and $\eta_{\min}$ (Equations 10 and 12), in our model. These parameters determine the maximum ice flow fluidity and can thus greatly impact the rate of mass loss during detachment. As shown in Figure 6b, for the same initial yield stress value (300 KPa), a combination of lower minimum stress $\tau_{\min}$ and minimum viscosity $\eta_{\min}$ values leads to a larger decrease in the rate of glacier mass. But this does not change the tipping point of glacier collapse, which is linked to ice flow dynamics and ice mechanical properties.

We should note that the yield stress of glacier ice is generally an unknown parameter and is highly heterogeneous in space. In this study, we approximate this tipping threshold value as a spatially uniform constant for the convenience of explaining the

https://doi.org/10.5194/egusphere-2025-659
Preprint. Discussion started: 31 March 2025

critical role ice strength plays in glacier detachment. The positive feedback in the weakening of ice strength beyond yield stress and in the rate-weakening basal friction probably contribute together to the collapse of the Sedongpu glacier in 2018. This suggest us to conduct consistent monitoring of heavy rainfall events and ice speed changes for suspiciously dangerous glaciers in the neighborhood regions, as subglacial water will lubricate bed, soften ice and accelerate ice flow, raising the probability of glacier collapse occurrence.

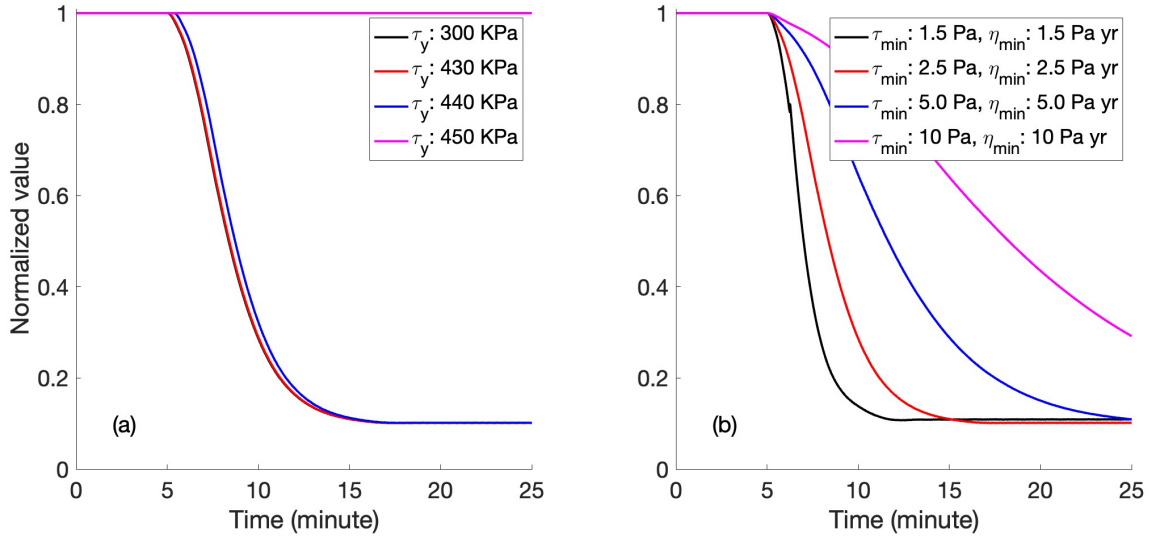

Figure 6. The sensitivity of mean ice thickness changes of Sedongpu to different initial yield stress values (a), model parameters $\tau_{\min}$ and $\eta_{\min}$ (b) during the 25 minute model time span. The detachment begins at minute 5.

5.4 The tipping processes of Sedongpu detachment

We can gain a further understanding of the detachment mechanism from Figure 7, which shows the dynamic changes of Sedongpu Glacier at three subsequent time steps after we activate the stiffness-slip coupling mechanism at time t_0. When we set the initial yield strength to 300 KPa, ice becomes yielded near the glacier head, terminus and at around km 1.3 at time t_0. Then, in the next time step, the entire glacier region becomes yielded, and ice flow accelerates remarkably. However, if we increase the initial yield strength values to 430 KPa and 500 KPa, we observe that the yielded regions near the head and terminus disappear after the velocity and ice thickness are updated in the next two time steps. When we set initial yield strength to 430 KPa, the entire glacier region becomes yielded at time step 3, and the ice velocity increases dramatically to nearly 100,000 m per hour, indicating the occurrence of glacier detachment. Conversely, when we set the initial yield strength to 500 KPa, the glacier remains stable in the next 3 time steps.

Previously, Kääb et al. (2018) and Gilbert et al. (2020) conducted in-depth and thorough studies of the Aru glacier collapse in 2016. They found the enormous Aru catastrophy was mainly controlled by multiple factors, e.g., deformable substrate,

https://doi.org/10.5194/egusphere-2025-659
Preprint. Discussion started: 31 March 2025

increased driving stress, temperate ice region and the connection to subglacial water. The transition from a slow ice movement feature to a catastrophic instability may have been underway for several months or years prior to the glacier collapse. Here in this study, we focus more on the dynamic instability during the abrupt glacier detachment, which can last only a few minutes. During this extreme rapid ice movement, we argue that the transition process from elastic to plastic deformation of ice is probably a non-negligible mechanism. This mechanism can lead to a positive feedback of ice flow acceleration and strength weakening and is traditionally not considered in the numerical simulations of glacier flow.

This glacier detachment tipping mechanism may also apply to other risky glaciers in the surrounding areas near the Sedongpu valley. For instance, the Zelongnong glacier (Fig. 1a) is considered as a potiential region where glacier detachment may occur. By assuming similar dynamic features as Sedongpu (e.g., similar initial yield strength), we can monitor the surface velocity field at Zelongnong and categorize its risk level by simulating its internal stress regime. This has remarkable scientific and engineering applications for large infrastructures in the local regions.

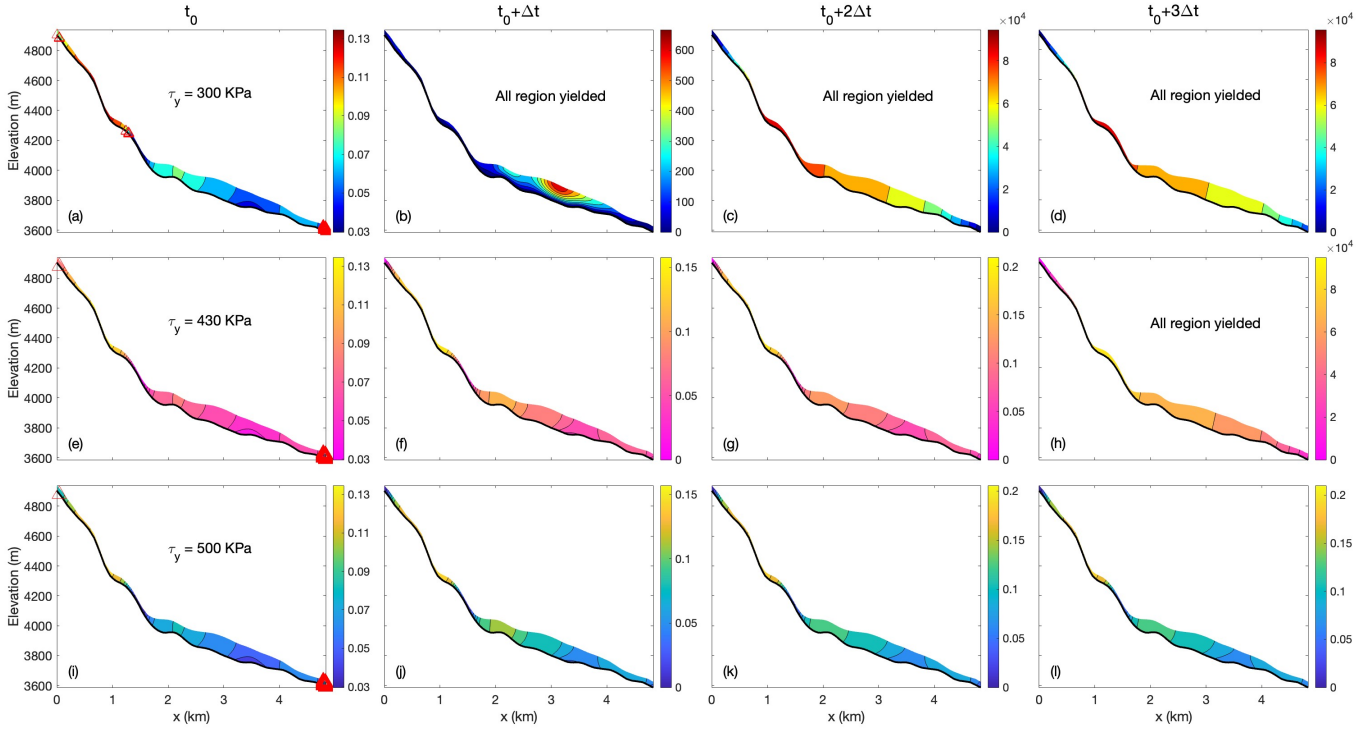

Figure 7. The changes of Sedongpu glacier velocity at 4 time steps after the ice stiffness-basal slip coupling mechanism is triggered. (a, b, c, d) initial yield strength is set as 300 KPa; (e, f, g, h) initial yield strength is set as 430 KPa; (i, j, k, l) initial yield strength is set as 500 KPa. The red triangles indicate the locations where ice gets yielded. The panels with "All region yielded" indicate that the entire glacier is yielded and ice flow accelerates drastically. The colorbars show the ice speed of Sedongpu Glacier with the unit of m yr^{-1}.

https://doi.org/10.5194/egusphere-2025-659
Preprint. Discussion started: 31 March 2025

5.5 Model limitations

Similar to Kääb et al. (2018), our modeling approach is still based on the framework of Glen's flow law but modified with a new stiffness-basal slip coupling scheme, where we assume the ice density remains constant during the detachment. Thus, it may not precisely capture the movement of the highly fratured detachment of the Sedongpu Glacier. Although the continuum modeling scheme (Bassis et al., 2021) we adopt here accounts for both flow and failure of ice, it cannot replace descrete methods to describe the ice collapsing processes. Additionally, we extract the glacier bed elevation by comparing the observed geometry before and after the detachment, which may introduce some uncertainties as the basal sediment of Sedongpu Glacier is very soft (Kääb et al., 2021) and the the subglacial geometry might have changed during the detachment. Furthermore, we do not consider the thermal coupling and basal hydrolodry schemes here, which may neglect some important physical mechanisms of glacier detachment. However, we argue that the coupling of basal hydrology and ice dynamics is probably insufficient to simulate these kinds of drastic ice flow changes like glacier detachment if we do not consider the internal changes of ice mechanical properties (e.g., yield stress). In this study, we have not taken a full consideration of the complex interactions between ice dynamics and bed properties (e.g., the Schoof sliding law and Iken's bound) (Helanow et al., 2020, 2021), but using a simpler sliding law (Eqn 13) to account for the rate-weakening effect of ice flow at the bed, which could also be improved in the future.

6 Conclusions

Glacier detachment is influenced by multiple factors, including glacier crevasses, meltwater, subglacial hydrology and basal slip properties. However, due to the lack of observational data and limitations in modeling capabilities, it is challenging to incorporate all these factors into simulations of glacier detachment. The primary goal of this study is to explore several key mechanisms that trigger glacier detachment, focusing mainly on the transitional process of internal stress within the glacier and the characteristics of basal sliding. We find that it is possible to capture the transition processes of the Sedongpu detachment from slow deformation to abrupt collapses by considering the changes in internal stress state of the glacier. By identifying some critical controlling factors, such as the yield strength of ice, in the ice flow model, we can recognize early warning signals of glacier detachment. We find that, for the Sedongpu Glacier, the initial yield strength is a tipping point beyond which the detachment will very likely to occur. In the near future, we may try to extend our current two dimensional study to three dimensions, and investigate further the relations between Iken's bound of glacier bed, basal sliding/hydrology and the changes of yield strength, which can help to advance our understandings of the glacier detachment mechanism and apply it to a larger spatial scale.

Code availability. The ice flow model PoLIM can be freely accessed at https://github.com/WangYuzhe/PoLIM-Polythermal-Land-Ice-Model

https://doi.org/10.5194/egusphere-2025-659
Preprint. Discussion started: 31 March 2025

Data availability. The model results (velocity, thickness, effective stress and viscosity) can be obtained from https://zenodo.org/records/15093450

Author contributions. TZ and WY conceived this study. TZ designed and constructed all model experiments. WY, YW, CZ and QL helped preparing the data of Sedongpu glacier. All authors contributed to the writing of the paper.

Competing interests. The authors declare no competing interests of this paper.

Acknowledgements. This work was supported by the National Key Research and Development Program of China (grant no. 2023YFF0805200), Open Research Fund of TPESER (Grant No. TPESER202203), the National Natural Science Foundation of China grant 42271133 and 42271134, the State Key Laboratory of Earth Surface Processes and Resource Ecology (2021-TS-06, 2021-KF-06, 2022-ZD-05), the Beijing Normal University Talent Introduction Project of China (12807-312232101), Basic Research Fund of CAMS (2023Z004), and Science and Technology Projects in the Tibet Autonomous Region (grant no. XZ202301ZY0028G).

https://doi.org/10.5194/egusphere-2025-659
Preprint. Discussion started: 31 March 2025

References

Acharya, A., Steiner, J. F., Walizada, K. M., Ali, S., Zakir, Z. H., Caiserman, A., and Watanabe, T.: Review article: Snow and ice avalanches in high mountain Asia – scientific, local and indigenous knowledge, Natural Hazards and Earth System Sciences, 23, 2569–2592, https://doi.org/10.5194/nhess-23-2569-2023, 2023.

Arthern, R. J. and Gudmundsson, G. H.: Initialization of ice-sheet forecasts viewed as an inverse Robin problem, Journal of Glaciology, 56, 527–533, 2010.

Arthern, R. J., Hindmarsh, R. C., and Williams, C. R.: Flow speed within the Antarctic ice sheet and its controls inferred from satellite observations, Journal of Geophysical Research: Earth Surface, 120, 1171–1188, 2015.

Bai, X. and He, S.: Dynamic process of the massive Aru glacier collapse in Tibet, Landslides, 17, 1353–1361, 2020.

Bassis, J., Berg, B., Crawford, A., and Benn, D.: Transition to marine ice cliff instability controlled by ice thickness gradients and velocity, Science, 372, 1342–1344, 2021.

Berthier, É. and Brun, F.: Karakoram geodetic glacier mass balances between 2008 and 2016: persistence of the anomaly and influence of a large rock avalanche on Siachen Glacier, Journal of Glaciology, 65, 494–507, 2019.

Blatter, H.: Velocity and stress fields in grounded glaciers: a simple algorithm for including deviatoric stress gradients, Journal of Glaciology, 41, 333–344, https://doi.org/10.3189/S002214300001621X, 1995.

Chen, C., Zhang, L., Xiao, T., and He, J.: Barrier lake bursting and flood routing in the Yarlung Tsangpo Grand Canyon in October 2018, Journal of Hydrology, 583, 124 603, 2020.

Cuffey, K. and Paterson, W.: The physics of glaciers, Elsevier, fourth edn., 2010.

Ding, C., Feng, G., Zhang, L., Shen, Q., Xiong, Z., and Liao, M.: The Precursory 3D Displacement Patterns and Their Implicit Collapse Mechanism of the Ice-Rock Avalanche Events Occurred in Sedongpu Basin Revealed by Optical and SAR Observations, Remote Sensing, 15, 2818, 2023.

Fugazza, D., Scaioni, M., Corti, M., D'Agata, C., Azzoni, R. S., Cernuschi, M., Smiraglia, C., and Diolaiuti, G. A.: Combination of UAV and terrestrial photogrammetry to assess rapid glacier evolution and map glacier hazards, Natural Hazards and Earth System Sciences, 18, 1055–1071, 2018.

Gao, H., Yin, Y., Li, B., Gao, Y., Zhang, T., Liu, X., and Wan, J.: Geomorphic evolution of the Sedongpu Basin after catastrophic ice and rock avalanches triggered by the 2017 Ms6. 9 Milin earthquake in the Yarlung Zangbo River area, China, Landslides, 20, 2327–2341, 2023.

Gilbert, A., Leinss, S., Kargel, J., Kääb, A., Gascoin, S., Leonard, G., Berthier, E., Karki, A., and Yao, T.: Mechanisms leading to the 2016 giant twin glacier collapses, Aru Range, Tibet, The Cryosphere, 12, 2883–2900, 2018.

Gilbert, A., Sinisalo, A., Gurung, T. R., Fujita, K., Maharjan, S. B., Sherpa, T. C., and Fukuda, T.: The influence of water percolation through crevasses on the thermal regime of a Himalayan mountain glacier, The Cryosphere, 14, 1273–1288, 2020.

Greve, R. and Blatter, H.: Dynamics of Ice Sheets and Glaciers, ISBN 3642034144, https://doi.org/10.1007/978-3-642-03415-2, 2009.

Helanow, C., Iverson, N. R., Zoet, L. K., and Gagliardini, O.: Sliding relations for glacier slip with cavities over three-dimensional beds, Geophysical Research Letters, 47, e2019GL084 924, 2020.

Helanow, C., Iverson, N. R., Woodard, J. B., and Zoet, L. K.: A slip law for hard-bedded glaciers derived from observed bed topography, Science Advances, 7, eabe7798, 2021.

Hu, W., Yao, T., Yu, W., Yang, W., and Gao, Y.: Advances in the study of glacier avalanches in High Asia, J. Glaciol. Geocryol, 40, 1141–1152, 2018.

https://doi.org/10.5194/egusphere-2025-659
Preprint. Discussion started: 31 March 2025

Kääb, A., Leinss, S., Gilbert, A., Bühler, Y., Gascoin, S., Evans, S. G., Bartelt, P., Berthier, E., Brun, F., Chao, W.-A., et al.: Massive collapse of two glaciers in western Tibet in 2016 after surge-like instability, Nature Geoscience, 11, 114–120, 2018.

Kääb, A., Jacquemart, M., Gilbert, A., Leinss, S., Girod, L., Huggel, C., Falaschi, D., Ugalde, F., Petrakov, D., Chernomorets, S., et al.: Sudden large-volume detachments of low-angle mountain glaciers–more frequent than thought?, The Cryosphere, 15, 1751–1785, 2021.

Kienholz, C., Rich, J., Arendt, A., and Hock, R.: A new method for deriving glacier centerlines applied to glaciers in Alaska and northwest Canada, The Cryosphere, 8, 503–519, 2014.

Kotlyakov, V. M., Rototaeva, O., and Nosenko, G.: The September 2002 Kolka glacier catastrophe in North Ossetia, Russian Federation: evidence and analysis, Mountain Research and Development, 24, 78–83, 2004.

Li, W., Zhao, B., Xu, Q., Scaringi, G., Lu, H., and Huang, R.: More frequent glacier-rock avalanches in Sedongpu gully are blocking the Yarlung Zangbo River in eastern Tibet, Landslides, pp. 1–13, 2022.

Liu, C., Lü, J., Tong, L., Chen, H., Liu, Q., Xiao, R., and Tu, J.: Research on glacial/rock fall-landslide-debris flows in Sedongpu basin along Yarlung Zangbo River in Tibet, Geology in China, 46, 219–234, 2019.

Luo, S., Xiong, J., Liu, S., Hu, K., Cheng, W., Liu, J., He, Y., Sun, H., Cui, X., and Wang, X.: New insights into ice avalanche-induced debris flows in southeastern Tibet using SAR technology, Remote Sensing, 14, 2603, 2022.

Messerli, A. and Grinsted, A.: Image georectification and feature tracking toolbox: ImGRAFT, Geoscientific Instrumentation, Methods and Data Systems, 4, 23–34, 2015.

Mishra, N. B., Miles, E. S., Chaudhuri, G., Mainali, K. P., Mal, S., Singh, P. B., and Tiruwa, B.: Quantifying heterogeneous monsoonal melt on a debris-covered glacier in Nepal Himalaya using repeat uncrewed aerial system (UAS) photogrammetry, Journal of Glaciology, 68, 288–304, 2022.

Montgomery, D. R., Hallet, B., Yuping, L., Finnegan, N., Anders, A., Gillespie, A., and Greenberg, H. M.: Evidence for Holocene megafloods down the Tsangpo River gorge, southeastern Tibet, Quaternary Research, 62, 201–207, 2004.

Pattyn, F.: Transient glacier response with a higher-order numerical ice-flow model, Journal of Glaciology, 48, 467–477, https://doi.org/10.3189/172756502781831278, 2002.

Salzmann, N., Kääb, A., Huggel, C., Allgöwer, B., and Haeberli, W.: Assessment of the hazard potential of ice avalanches using remote sensing and GIS-modelling, Norsk Geografisk Tidsskrift-Norwegian Journal of Geography, 58, 74–84, 2004.

Thøgersen, K., Gilbert, A., Schuler, T. V., and Malthe-Sørenssen, A.: Rate-and-state friction explains glacier surge propagation, Nature communications, 10, 2823, 2019.

Wang, Y., Zhang, T., Ren, J., Qin, X., Liu, Y., Sun, W., Chen, J., Ding, M., Du, W., and Qin, D.: An investigation of the thermomechanical features of Laohugou Glacier No. 12 on Qilian Shan, western China, using a two-dimensional first-order flow-band ice flow model, The Cryosphere, 12, 851–866, https://doi.org/10.5194/tc-12-851-2018, 2018.

Wang, Y., Zhang, T., Xiao, C., Ren, J., and Wang, Y.: A two-dimensional, higher-order, enthalpy-based thermomechanical ice flow model for mountain glaciers and its benchmark experiments, Computers & Geosciences, 141, 104 526, https://doi.org/https://doi.org/10.1016/j.cageo.2020.104526, 2020.

Yang, W., Yao, T., Guo, X., Zhu, M., Li, S., and Kattel, D. B.: Mass balance of a maritime glacier on the southeast Tibetan Plateau and its climatic sensitivity, Journal of Geophysical Research: Atmospheres, 118, 9579–9594, 2013.

Yang, W., Wang, Z., An, B., Chen, Y., Zhao, C., Li, C., Wang, Y., Wang, W., Li, J., Wu, G., et al.: Early warning system for ice collapses and river blockages in the Sedongpu Valley, southeastern Tibetan Plateau, Natural Hazards and Earth System Sciences, 23, 3015–3029, 2023.

https://doi.org/10.5194/egusphere-2025-659
Preprint. Discussion started: 31 March 2025

Zhang, T., Xiao, C., Colgan, W., Qin, X., Du, W., Sun, W., Liu, Y., and Ding, M.: Observed and modelled ice temperature and velocity along the main flowline of East Rongbuk Glacier, Qomolangma (Mount Everest), Himalaya, Journal of Glaciology, 59, 438–448, https://doi.org/10.3189/2013JoG12J202, 2013.

Zhang, T., Wang, W., Shen, Z., and An, B.: Increasing frequency and destructiveness of glacier-related slope failures under global warming, Science Bulletin, 69, 30–33, 2024.